Asian Journal of Chemistry; Vol. 35, No. 6 (2023), 1391-1400

ASIAN JOURNAL OF CHEMISTRY

https://doi.org/10.14233/ajchem.2023.27799

Surfactant Assisted Synthesis of $BiVO_4$ by Low Temperature Solvothermal Method: Effect of Calcination for Photocatalytic Activity

REHABOTH NISSI J.[1], B. VIDHYA[1,*] and J. SURYAKANTH[2]

[1]Department of Physics, Karunya Institute of Technology and Sciences, Coimbatore-641114, India
[2]Department of Physics, KPR Institute of Engineering and Technology, Arasur, Coimbatore-641407, India

*Corresponding author: E-mail: vidhyabhojan@gmail.com

Received: 19 March 2023; *Accepted*: 18 April 2023; *Published online*: 27 May 2023; AJC-21254

A visible light active semiconductor photocatalyst, $BiVO_4$ was synthesized through low temperature solvothermal method in hot air oven followed by calcination. To enhance the degradation rate surfactants were employed, which shows the better degradation for calcinated hexamine added $BiVO_4$, *i.e.* 74% of methylene blue was degraded in 180 min in visible light irradiation. The result is correlated with lower band gap energy value, *i.e.* 2.07 eV and lower photoluminescence emission spectra intensity. It was observed the variation in surface morphology of the prepared samples. The specific surface area of calcinated hexamine added $BiVO_4$ was analyzed by BET analysis. All the prepared samples showed higher absorption in UV-visible region. The FTIR confirmed the presence of hexamine in the calcinated hexamine sample.

Keywords: $BiVO_4$, Calcination, Hexamine, Low temperature, Methylene blue.

INTRODUCTION

Environmental pollution and energy crisis are greatly increasing with the advancement in industrialization. It is significant and also challenging to eliminate the sewage and toxic organic chemicals released from several industrial processes. Utilization of sunlight is an effective approach in the decomposition of organic contaminants [1]. Elimination of organic dyes from wastewater through the photocatalytic process is one of the most simple, effective and economical pathway [2]. Semiconductor photocatalysts with high photocatalytic activity have gained a great attention [3]. During the past decades, TiO_2 based photocatalysts have been extensively studied and it has many advantages towards photocatalysis. But the range of frequencies works on is limited to the UV region [4]. To utilize solar light effectively, it is highly desirable to develop novel semiconductor materials with higher photocatalytic activity under visible light irradiation [5]. Several studies proposed visible region active and narrow band gap semiconductor photocatalyst such as CdS, Bi_2WO_6, Bi_2S_3, $BiVO_4$, *etc*. Among these, $BiVO_4$ has attracted special interest because of its enhanced photocatalytic activity under visible light irradiation [6].

$BiVO_4$ exists in three different polymorphs *i.e.* monoclinic scheelite, tetragonal scheelite and tetragonal zircon. Monoclinic scheelite $BiVO_4$ exhibits higher photocatalytic activity due to its narrow band gap than the other two crystal phases. Whereas, the domination of insufficient charge separation of the charge carrier reduces the photocatalytic activity of $BiVO_4$. In order to enhance the photocatalytic activity, different synthesis routes resulting in different morphology and facet dependent properties were developed [7]. Among them, hydrothermal method has attracted great attention due to its simplicity, effectiveness in production and controllable morphology in an environmentally approachable way. In this approach numerous parameters such as concentration, precursor nature, precursor solution pH, hydrothermal time and temperature can be controlled to get the desired crystal structure and morphology of the material [8]. Wang *et al.* [9] adapted the hydrothermal method with low temperature and synthesized $BiVO_4$ with co-exposed facet and obtained 70% degradation of methylene blue dye. To prepare $BiVO_4$ with regular morphology, surfactant agents or template-directing reagents are also employed in recent years [10]. The surfactant assisted preparation of photocatalyst is an effective and facile approach in regulating the surface porosity [11] and

obtaining different morphologies. Further, it can regulate micro-environment of reaction and adjust the growth direction of the nanoparticles, leading to the formation of desired morphology [12]. It also influences the energy band structure to improve the catalytic activity [13]. The surfactants commonly used in the synthesis of $BiVO_4$ with different preparation methods are PVP, PVA, PEG, EDTA, SDS, *etc*. [14]. In present study, hexamine, PEG, PVA and PVP were chosen as surfactants based on literatures.

Hexamine acts as a shape inducing polymer and helps in the faster elimination of the gaseous products and cause more particles to interact with each other [15]. It is a hydroxyl anion generating agent and the hydrolysis of hexamine proceeds above 70 ºC. As the amount of hexamine increases the crystallite size also increases, the lesser amount of hexamine results in lesser specific area [16]. PEG is suitable structure directing agent due to its high solubility in water and organic solvents and thermal decomposition. It suppresses the crystal growth and enhances the specific surface area [14,17]. The special restriction field for BiO^+ and VO_3^- ions provided by the PEG and its high viscosity prevents the large particle formation and results in uniform particle formation [18]. PVA is a low-cost highly water soluble and a stable surfactant, which forms a protective layer for reinforcement bonding of a material [19]. PVP serves as the reductant to promote the formation and *in situ* growth of $BiVO_4$. It can also induce SPR effect in the composite [20]. PVP, a negatively charged surfactant coordinates with Bi^{3+} ions and forms the complex Bi^{3+}-PVP in the solution and controls the reaction to obtain the required morphology [21,22].

On the other side calcination is reported to influence the crystallinity, structure and morphology of $BiVO_4$ resulting in better performance. Hence, based on the above literatures, this work throws light on understanding the effect of different surfactants followed by conventional calcination to the most promising visible light active catalyst $BiVO_4$ [23].

EXPERIMENTAL

The highest grade chemicals like bismuth nitrate pentahydrate ($Bi(NO_3)_3{\cdot}5H_2O$, HiMedia), ammonium metavanadate (NH_4VO_3, LOBA Chemie), acetic acid (Sigma Life Science), ethanol (LOBAGENS, China), aq. ammonia (Sigma Life Science), polyvinylpyrrolidone (PVP), polyvinylalcohol (PVA), hexamethylenetetramine (hexamine), polyethylene glycol (PEG), ethylenediaminetetraacietic acid (EDTA) was purchased from Sigma Life Science, while 1,4-benzoquinone (BQ), isopropyl alcohol (IPA) was purchased from LOBA Chemie and used as such.

Preparation: Bismuth nitrate pentahydrate ($Bi(NO_3)_3{\cdot}5H_2O$, 0.97 g) was stirred in the solution of acetic acid:ethanol: distilled water (1:1:3) and also 0.25 g NH_4VO_3 was dissolved separately in ammonia solution (3:1). The solutions were stirred separately for 20 min, after which both the solutions were mixed together and stirred for few minutes followed by the addition of 0.25 g of polymer and finally stirred further for 30 min. The stirred solution was transferred to the autoclave and kept in the hot air oven for 3 h at 80 ºC. The final product was filtered, washed with distilled water and ethanol three times and dried overnight in the hot air oven. The final yellow powder was calcinated (500 ºC in muffle furnace for 3 h). The prepared samples were identified as UX (U = Untreated, X = bare, hexamine added, PEG added, PVA added and PVP added) for as prepared samples and CX (C = calcination) for calcinated samples.

Photocatalytic studies: The photocatalytic behaviour of the as-prepared samples was evaluated by the degradation of methylene blue (MB), a synthetic basic dye. Typically 20 mg of photocatalyst was dispersed in 100 mL of aqueous solution of MB dye. The suspension was stirred in dark condition for 30 min to establish the adsorption-desorption equilibrium between the dye solution and the photocatalyst. A 250 W low voltage halogen lamp was used as the visible light source. After 30 min stirring in dark condition the light source was switched on and then irradiated upto 150 min. During the reaction, 7 mL of suspension was collected and analyzed for the absorbance intensity. The absorbance intensity was recorded by the UV-Vis-NIR spectrophotometer at the wavelength of 663 nm. The suspension was collected at a time interval of 30 min.

Characterization: The crystalline phase of as-prepared samples was evaluated by X-ray diffractometer (XRD, Shimadzu, Japan, model: XRD-6000) with Cu$K\alpha$ radiation (λ = 0.15406 nm). The range of 2θ was maintained as 5º to 80º. The morphology of the samples was analyzed by scanning electron microscope (SEM, JEOL, Japan, model: JSM 6390). UV Vis diffuse reflectance spectra (DRS) was determined by UV-Vis spectrophotometer (JASCO UV, model: V-770), whereas the photoluminescence data was recorded by spectrofluorophotometer (Shimadzu, model: RF - 5301PC). The adsorption intensity of methylene blue dye was evaluated by UV-Vis-NIR spectrophotometer (JASCO, model: V-670) and Fourier transform infrared (FTIR) spectra was analyzed to detect the presence of bonding and hexamine in the prepared samples. The surface pore volume and pore size were evaluated by BET analysis with nitrogen adsorption/desorption analyzer using nitrogen gas.

RESULTS AND DISCUSSION

XRD studies: The crystal structure of as-prepared samples was determined by XRD and the obtained diffraction pattern is exhibited in Fig. 1a and 1c. The narrow diffraction peaks of the prepared samples confirmed the crystalline nature of the samples. The 2θ values from XRD results are matched with the standard JCPDS card no. 83-1699. The observed peaks are associated with the monoclinic phase of $BiVO_4$. The absence of other impurity peaks confirms the phase purity of the prepared samples [24]. According to literature, monoclinic phase of $BiVO_4$ shows a better degradation than the other phases [7]. From Fig. 1a and 1c, it is observed that the intensity of the diffraction peaks varies with different surfactants. In untreated samples, the intensity of the samples is lower than untreated $BiVO_4$ (UB). But in calcination processed samples, CG and CP has higher intensity and CH and CA has lower intensity than CB. It implies that the addition surfactant broadens the peaks and calcination process affects the intensity of peaks [25]. The crystallite size, dislocation density and micro-strain were calculated using the Debye- Scherrer's equation:

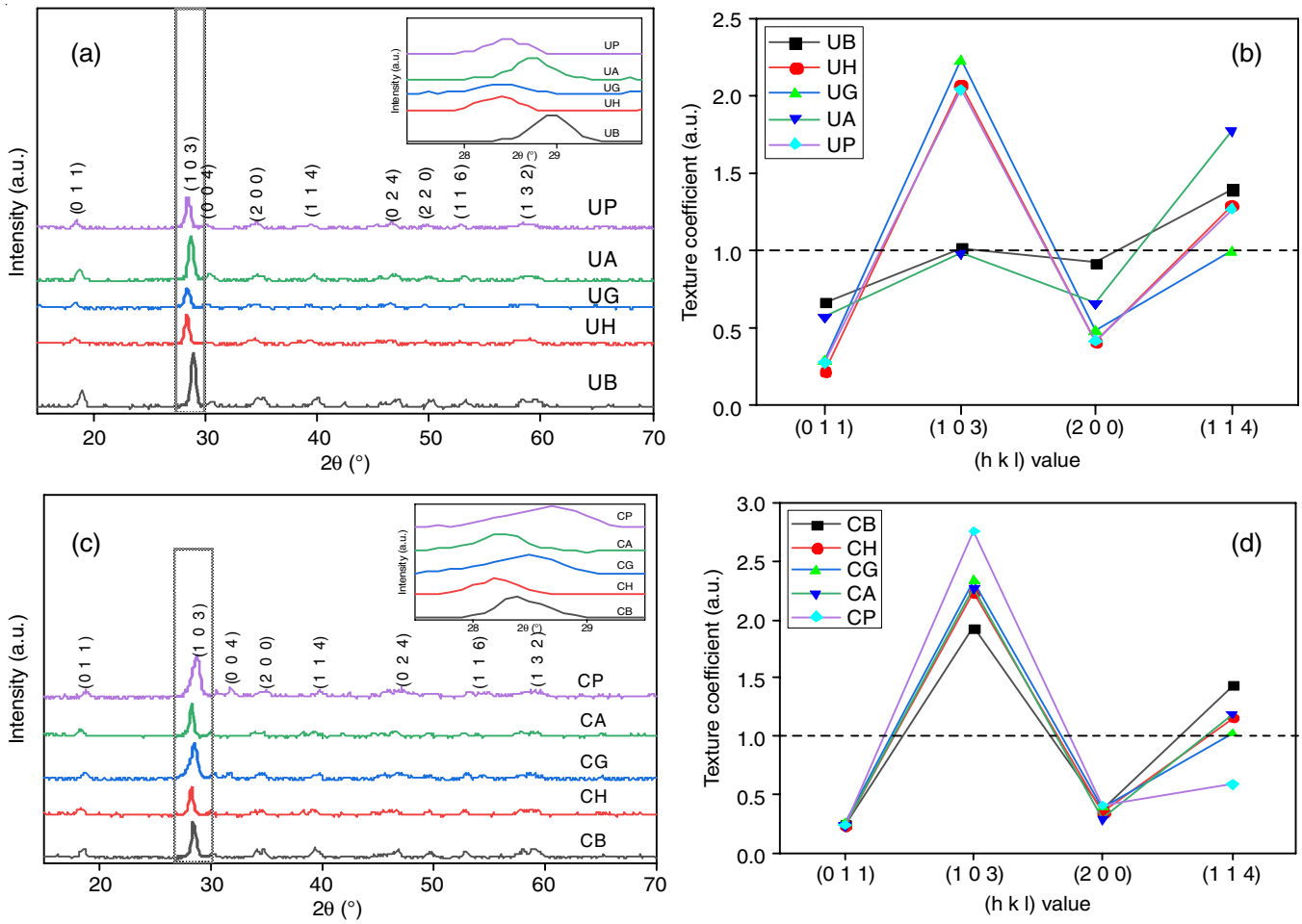

Fig. 1. XRD diffraction peaks of the prepared samples (left figure) and the texture coefficient of the prepared samples (right figure). UB – untreated $BiVO_4$, UH – untreated hexamine added $BiVO_4$, UG – untreated PEG added $BiVO_4$, UA – untreated PVA added $BiVO_4$, UP – untreated PVP added $BiVO_4$, CB – calcinated $BiVO_4$, CH – calcinated hexamine added $BiVO_4$, CG – calcinated PEG added $BiVO_4$, CA – calcinated PVA added $BiVO_4$, CP – calcinated PVP added $BiVO_4$

$$D = \frac{k\lambda}{\beta\cos\theta} \quad (1)$$

$$\delta = \frac{1}{D^2} \quad (2)$$

$$\mu = \frac{\beta\cos\theta}{4} \quad (3)$$

where, D is the crystallite size in nm, k is the shape factor (0.9 for cubic structure), λ is the wavelength of the incident beam (1.5406 Å), β is full width half maximum (FWHM) of the considered peak position, θ is the peak position, δ is the dislocation density in m^{-2} and μ is the micro-strain [26]. The crystallite size, dislocation density and micro strain are calculated by considering the highest intensity peak.The calculated crystallite size, dislocation density and micro strain are tabulated in Table-1.

In untreated samples, the crystallite size got decreased after the addition of surfactant and after the calcination process, the crystallite size decreased for CG and CP and increased for CH and CA than CB. The crystallite size of the samples CB, CG and CP decreased than UB, UG and UP and increased in CH and CA than UH and UA after the calcination process. The dislocation density and micro-strain is inversely proportional to crystallite size. The decrease in dislocation density and micro strain induces the crystallite size [26].

TABLE-1
CALCULATED RESULTS OF THE CRYSTALLITE SIZE, DISLOCATION DENSITY AND MICRO STRAIN OF THE PREPARED SAMPLES

Sample	Crystallite size (D) (nm)	Micro strain (μ) (10^{-3})	Dislocation (δ) (10^{15})
Untreated $BiVO_4$ (UB)	18	1.8966	2.9939
Calcinated $BiVO_4$ (CB)	15	2.3019	4.4101
Untreated hexamine (UH)	15	2.2998	4.4016
Calcinated hexamine (CH)	16	2.1681	3.9119
Untreated PEG (UG)	12	2.8372	6.6992
Calcinated PEG (CG)	10	3.4448	9.8759
Untreated PVA (UA)	16	2.2234	4.1143
Calcinated PVA (CA)	17	2.0642	3.5462

To evaluate the degree of preferential orientation of the plane, texture coefficient was calculated. The texture coefficient provides the information about the preferential or random growth of the particles. It was calculated using eqn. 2:

$$T_c = \frac{I_{(hkl)} / I_{0(hkl)}}{\frac{1}{N}\left[\sum I_{(hkl)} / I_{0(hkl)}\right]} \quad (4)$$

where T_c is the texture coefficient of the plane, $I_{(hkl)}$ denotes the measured peak intensity of the corresponding (*h k l*) plane, $I_{0(h\ k\ l)}$ is the standard intensity (reference intensity) of that considered (*h k l*) plane from JCPDS card 83-1699 and N is the number of reflections considered for the analysis [27]. Four most preferential orientations of the crystal *viz.* (0 1 1), (1 0 3), (2 0 0) and (1 1 4) planes are considered for the calculation of texture coefficient. The standard value for the texture coefficient along the abundant crystal growth is 1 [28]. The value of texture coefficient lower than 1 indicates the lower degree of favoured preferential orientation along that particular plane and higher than 1 describes the higher degree of favoured orientation along that particular plane. It implies the abundance of the crystal orientation towards that facet direction [29]. The calculated texture coefficient is given in Table-2 and the results are plotted in the graph and exhibited in Fig. 1b and 1d.

TABLE-2
CALCULATED RESULT OF THE TEXTURE COEFFICIENT OF THE PREPARED SAMPLES

Sample	(0 1 1)	(1 0 3)	(2 0 0)	(1 1 4)
Untreated $BiVO_4$ (UB)	0.6698	1.0133	0.9206	1.3962
Calcinated $BiVO_4$ (CB)	0.2485	1.9301	0.3793	1.4418
Untreated hexamine (UH)	0.2266	2.0715	0.4098	1.2921
Calcinated hexamine (CH)	0.2442	2.2336	0.3581	1.1638
Untreated PEG (UG)	0.2953	2.2241	0.4836	0.9967
Calcinated PEG (CG)	0.2599	2.3274	0.3908	1.0217
Untreated PVA (UA)	0.5758	0.9841	0.6644	1.7761
Calcinated PVA (CA)	0.2378	2.2660	0.3009	1.1952
Untreated PVP (UP)	0.2787	2.0381	0.4176	1.2654
Calcinated PVP (CP)	0.2439	2.7539	0.4106	0.5914

From the calculated results after the calcination, the orientation of pure $BiVO_4$ (UB) and PVA added $BiVO_4$ (UA) shows the transformation to (1 0 3) plane from (1 1 4) plane and all the other prepared samples shows the orientation along the (1 3 0) plane. The highest texture coefficient value correlates the higher number of grains towards (1 0 3) plane. Hence, it is inferred that the temperature affects the preferential orientation crystal growth [27]. The reduction in the (1 1 4) plane may be associated with the minimization in surface energy and strain energy [29].

SEM studies: The particle distribution and crystal shape can be observed through the SEM images (Fig. 2). The surface morphology of the prepared samples varies with the addition of surfactants to the pure $BiVO_4$ (UB). The SEM images proved that the presence of the surfactants affected its morphology. It can observe tiny rod like structure in as prepared sample UB. The surfactants has formed tiny lump like structure on the surface of the material and the nanoparticles produces cluster like structures after the calcination process. The surfactants play a vital role in modifying the morphology of the samples [29,30].

Photocatalytic activity: The photocatalytic activity of as-prepared nanoparticles was assessed by estimating the decolorization of synthetic dye in an aqueous solution. Herein, methylene blue dye was adopted as a probe dye to study the photocatalytic activity under the visible light exposure. The graph of C/C_0 is exhibited in Fig. 3. The UB shows only 48% of degradation efficiency of dye in 180 min of visible light irradiation. After the calcination, not all the samples showed improved degradation but the CH sample shows enhancement in the degradation rate *i.e.* from 23% to 74%. It is observed that calcination did not help to improve the degradation rate in all the calcinated samples. Although the morphology was altered, the degradation rate was not similarly impacted. Fig. 3c exhibits the reduction in wavelength from 660 nm to 632 nm as the degradation of methylene blue occurs with the increase in time of exposure [31].

The photodegration kinetics of methylene blue dye solution for the prepared photocatalysts was evaluated using the pseudo first order kinetic equation [32]. The pseudo-first order kinetic equation is described by the Langmuir-Hinshelwood model and the equation is given below:

$$\ln\frac{C}{C_0} = kt \quad (5)$$

where, k stands for the pseudo first order reaction rate constant, t is the time of irradiation, C is the intensity of concentration of the methylene blue solution after the irradiation of visible light in t time and C_0 is the initial intensity of concentration of methylene blue solution before the irradiation of visible light. The value of k can be estimated by the tangent to the line of best fit slope of the plot ln (C/C_0) *versus* t and results are shown in Table-3. The graph is exhibited in the inset of C/C_0 graph and is displayed in Fig. 3 [33]. Among all the samples CH has the highest rate constant. This can be unfolding the consequence of the appropriate morphology of the samples under the prepared condition [34]. Herein, the UA and CH samples have higher degradation rate among untreated samples and calcination processed samples, also UA and CH both have same crystallite size (from XRD analysis result). And this might be a reason in increasing degradation than other samples.

TABLE-3
RESULTS OF THE DEGRADATION AND RATE CONSTANT OF THE PHOTOCATALYSTS

Sample	Degradation rate (%)	Kinetic rate constant ($\times 10^{-3}$)
Untreated $BiVO_4$ (UB)	48	4.5
Calcinated $BiVO_4$ (CB)	28	2.3
Untreated hexamine (UH)	23	1.7
Calcinated hexamine (CH)	74	9.1
Untreated PEG (UG)	39	3.4
Calcinated PEG (CG)	32	2.6
Untreated PVA (UA)	61	6.8
Calcinated PVA (CA)	51	5.1
Untreated PVP (UP)	26	1.8
Calcinated PVP (CP)	46	4.0

Reusability and radical species test: The reusability of a photocatalyst is also an important factor for the actual application of the photocatalyst [35]. Through a recycling test of the photodegradation under visible light, the sample (CH) that

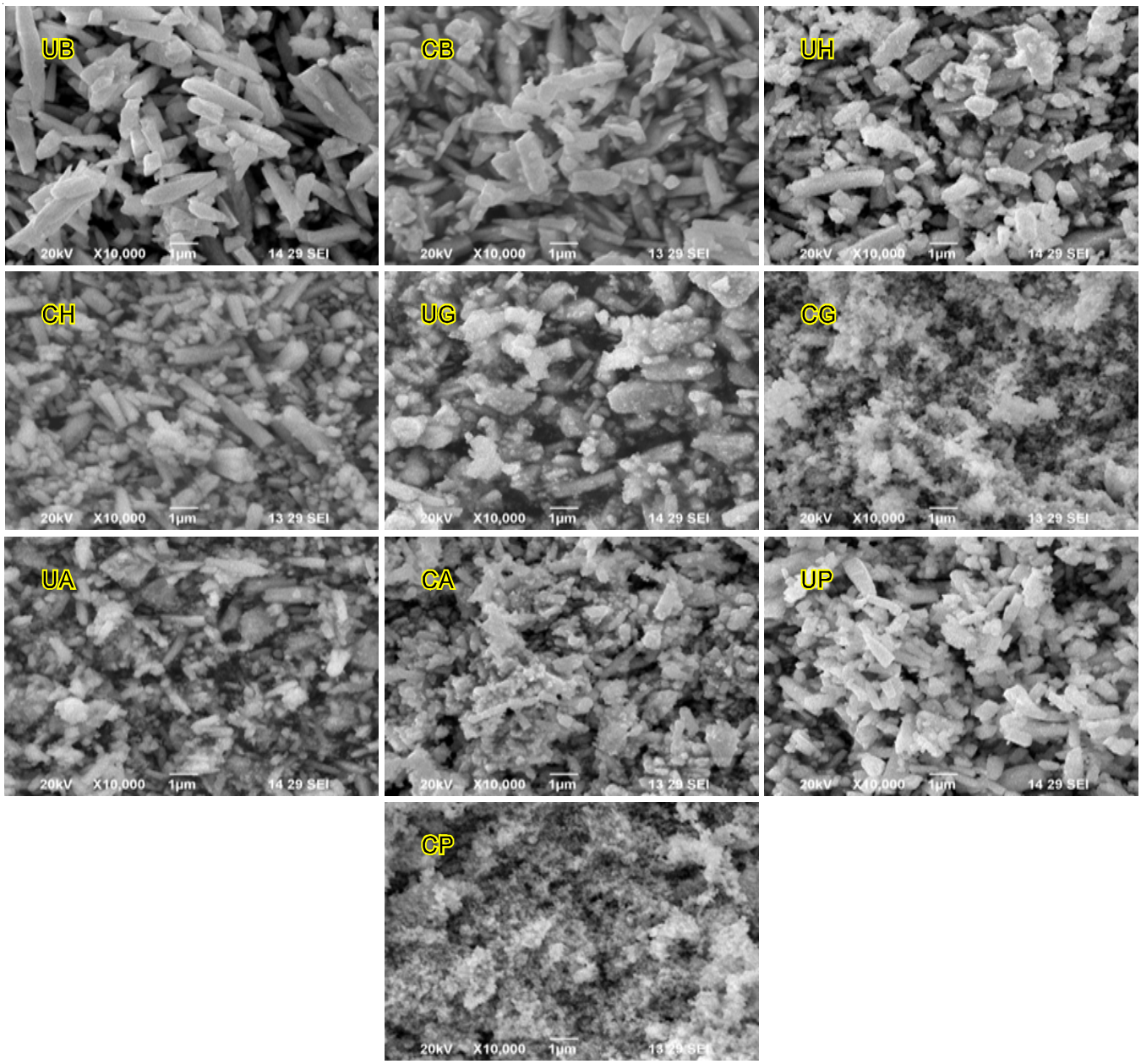

Fig. 2. SEM images of the prepared samples, UB – untreated $BiVO_4$, CB – calcinated $BiVO_4$, UH – untreated Hexamine added $BiVO_4$, CH – calcinated hexamine added $BiVO_4$, UG – untreated PEG added $BiVO_4$, CG – calcinated PEG added $BiVO_4$, UA – untreated PVA added $BiVO_4$, CA – calcinated PVA added $BiVO_4$, UP – untreated PVP added $BiVO_4$, CP – calcinated PVP added $BiVO_4$

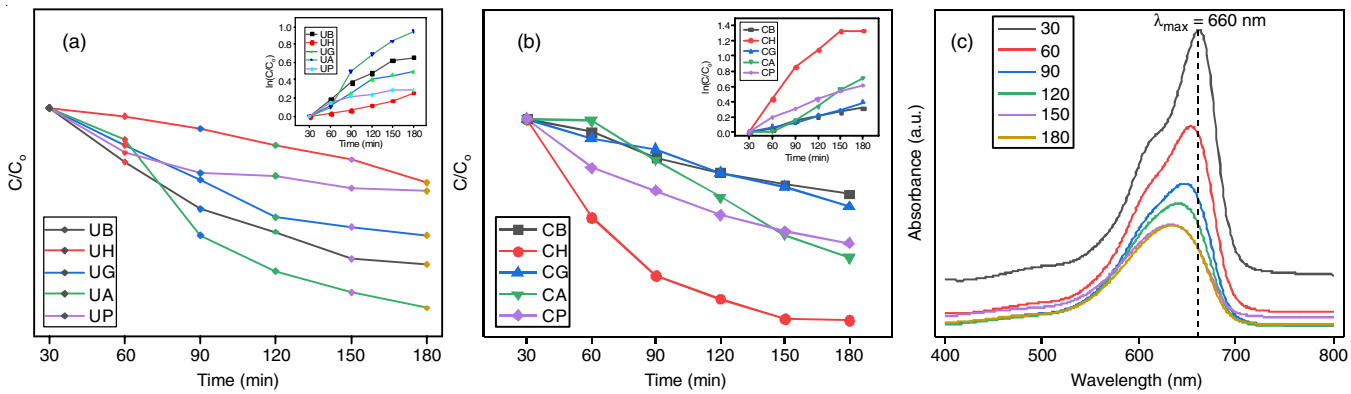

Fig. 3. Graph of C/C_o *versus* time and inset graph of ln (C/C_o) *versus* time

shown better degradation among all the generated samples is taken into consideration for the reusability study [36]. The recycling test runs with 30 min adsorption in dark and 150 min in the light irradiation in each cycle for the decomposition of methylene blue dye. The reusability cycle results are shown in Fig. 4a. They showed only 10% decrease after third cycle and this may be due to the loss of photocatalyst during the cycle. And it reveals the reusability and stability of the photocatalyst for the degradation process under visible light irradiation [37].

To determine the reactive species produced during the photocatalytic process, active species trapping experiment was performed for the CH sample. It is done with three different scavengers, *e.g.* 1,4-benzoquinone (BQ), ethylenediamine tetra-acetic acid (EDTA) and isopropyl alcohol (IPA) to quench super oxide radical ($O_2^{\bullet-}$), hole (H^+) and hydroxyl ($^\bullet OH$) radicals, respectively [38]. Fig. 4b shows the results of scavenger test for the sample. The degradation of methylene blue dye with the scavenger is in the order BQ > EDTA > IPA. Because photo-degradation of methylene blue dye was inhibited most significantly in the presence of BQ, it can be safely concluded that superoxide radicals play a crucial part in this process ($O_2^{\bullet-}$) [39].

Optical studies: The photocatalytic property of as-prepared sample was examined using UV-Vis diffuse reflectance spectra (UV-Vis DRS). The UV-Vis DRS has been analyzed in the range of 200 to 800 nm and is displayed in Fig. 5. All the catalysts show a strong absorption in both UV and visible region of the electromagnetic spectrum and it indicates the possibility of photocatalytic response in sunlight. The steep shape of the optical absorbance curve shows the transition of band gap is responsible for the visible light absorption [40]. The absorption intensity was found to be higher in UA and CP samples. The higher degradation in UA may be due to the better absorption of dye (from photocatalysis analysis result). The band gap energy was determined by using Tauc's equation as below:

$$\alpha h\nu = A(h\nu - E_g)^{n/2} \quad (6)$$

where α, h, ν, A, E_g and n represents the absorption coefficient, Plank's constant, the incident light frequency, a constant, the band gap energy and an integer, respectively. The integer n depends on the characteristics of transition in a semiconductor [41] *i.e.* n = 1 in direct transition and n = 4 for indirect transition. For the prepared samples n = 1 as they are direct transition

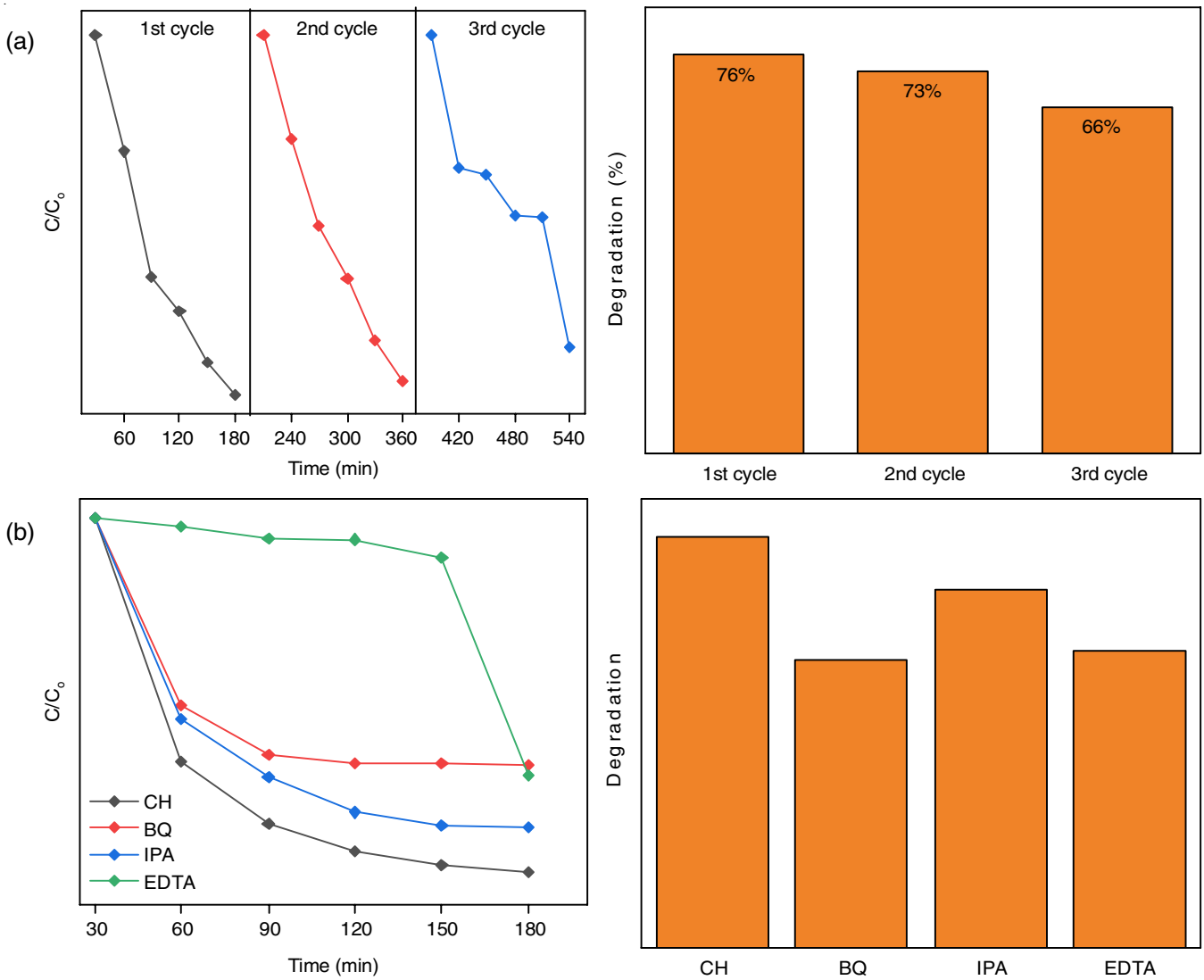

Fig. 4. The reusability test cycle and the scavenger analysis graph of CH, (a) reusability test cycle, (b) scavenger analysis

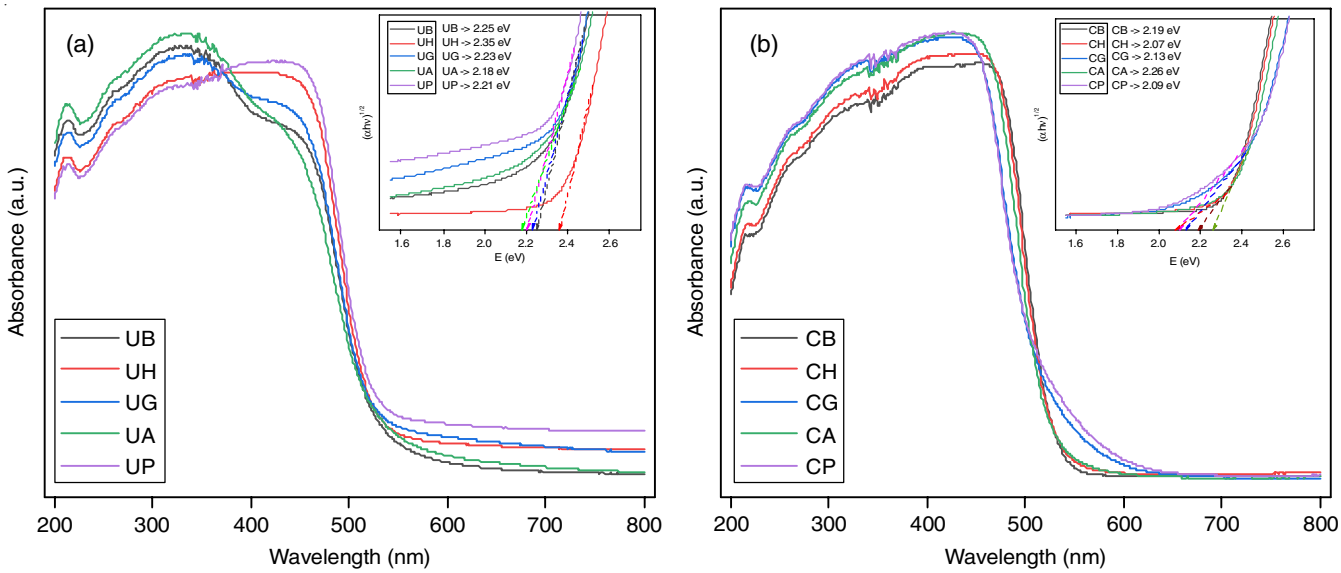

Fig. 5. The graph of absorption and the Tauc's plot (in inset) (a) untreated samples, (b) calcinated samples

photocatalyst. The band gap energy of the photocatalysts has been evaluated by the intercept to the $(\alpha h\nu)^{1/2} = 0$ axis in the Tauc's plot of $(\alpha h\nu)^{1/2}$ *versus* radiation energy (eV) [42]. The estimated band gap energy is given in Table-4. The photo-degradation efficiency is different for different samples though they show almost identical absorption efficiency (Fig. 5) and hence it infers that the visible light response of the prepared materials is independent of the photocatalytic performance efficiency [41]. The conduction band and valence band of the prepared samples were calculated using the following equations:

$$E_{VB} = X - E_e + 0.5E_g \quad (7)$$

$$E_{CB} = E_{VB} - E_g \quad (8)$$

where E_{VB}, E_{CB}, E_g, E_e and X are valence band potential, conduction band potential, band gap energy, the free electron energy based on the hydrogen scale (4.5 eV) and the arithmetical mean of the absolute electronegativity of the component atoms of the semiconductor respectively, and for $BiVO_4$ it is 6.0349 eV [39].

Photoluminescence studies: Photoluminescence (PL) spectra is evaluated to detect the photoinduced charge carriers transfer efficiency and displayed in Fig. 6. The UA and UB samples showed better degradation among the prepared and calcinated samples and UB is considered for the comparision with other 2 samples. The low intensity of PL spectra represents the higher photocatalytic performance [43]. In Fig. 6, it was observed that CH shows the lowest intensity and has the better degradation among the prepared samples (from photocatalytic activity results). Only the UB shows the intensity peak at 660 nm and other 2 samples at 494 nm in the PL spectra. After the addition of surfactant and the calcination process, the blue shift can be observed in the PL spectra. The blue shift of wavelength in the plot can be related to the presence of oxygen vacancies of the material. The vacancies are induced by the incomplete oxidation in the material during the recombination of hole and electron formed in the O2p band and V3d band of $BiVO_4$, respectively. And these oxygen vacancies help in enhancing the photocatalytic activity by decomposing the organic contaminants [44,45].

TABLE-4
CALCULATED RESULT OF VALENCE BAND AND CONDUCTION BAND VALUE AND THE ESTIMATED ENERGY BAND GAP VALUE

Sample	Energy band gap (eV)	Valence band value (eV)	Conduction band value (eV)
Untreated $BiVO_4$ (UB)	2.25	3.03	0.78
Calcinated $BiVO_4$ (CB)	2.19	3.01	0.82
Untreated hexamine (UH)	2.35	3.08	0.73
Calcinated hexamine (CH)	2.07	2.94	0.87
Untreated PEG (UG)	2.23	3.02	0.79
Calcinated PEG (CG)	2.13	2.97	0.84
Untreated PVA (UA)	2.18	2.99	0.81
Calcinated PVA (CA)	2.26	3.04	0.78
Untreated PVP (UP)	2.21	3.01	0.80
Calcinated PVP (CP)	2.09	2.95	0.86

BET analysis: Bulk properties of the synthesized samples *i.e.* the specific surface area and pore size of the photocatalysts was evaluated using the BET multilayer theory of adsorption-desorption experiment by the adsorption of liquid nitrogen at 73 K. The UB, UA and CH samples were considered due to their higher degradation efficiency among all the prepared samples. The pore size and specific surface area of the photocatalysts are also the important factors affecting the photocatalytic performance [46]. The N_2 adsorption-desorption isotherm curve of the photocatalysts and the corresponding BJH pore size distribution plot (inset) are shown in Fig. 7. From the distinguished hysteresis loop of the samples, the rapid increment can be observed in the higher region of BET isotherm plot and causes the adsorption-desorption hysteresis phenomenon *i.e.* to say that the adsorption curve is formed below the desorption curve forming a hysteresis loop. In the range of 0.7-0.9 P/P_0, the rapid increment occurred as a result of capillary condensation that took place in the mesoporous structures [46,47]. According to IUPAC size classification the BET isotherm graphs of UB

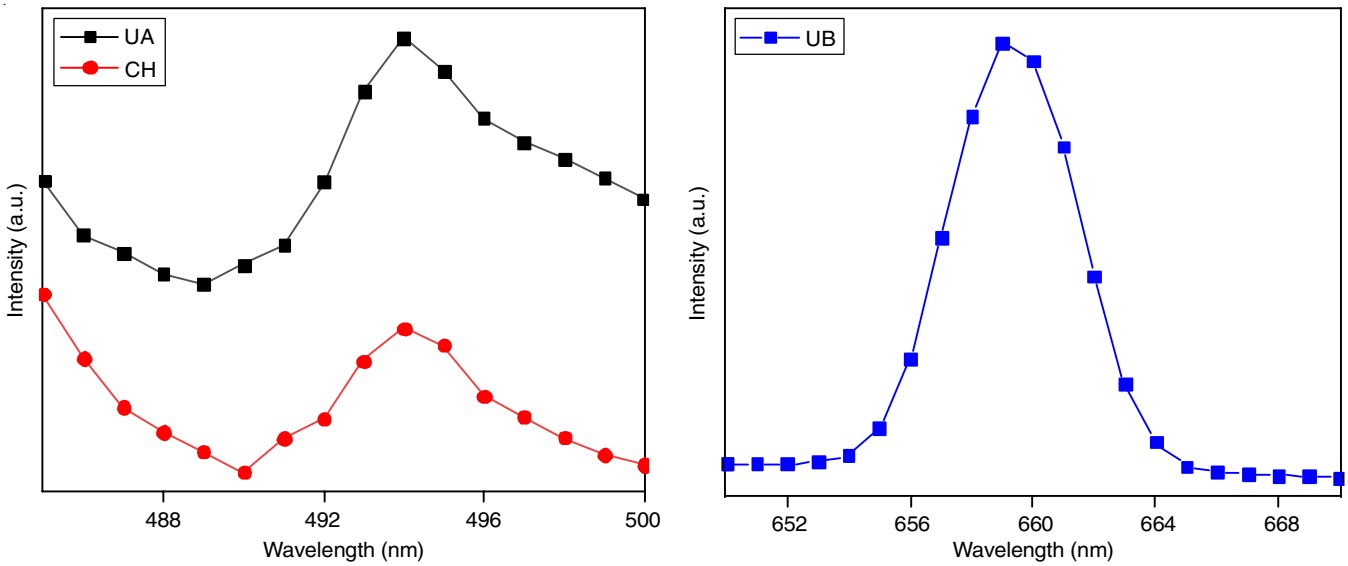

Fig. 6. The photoluminescence spectra of the prepared photocatalyst

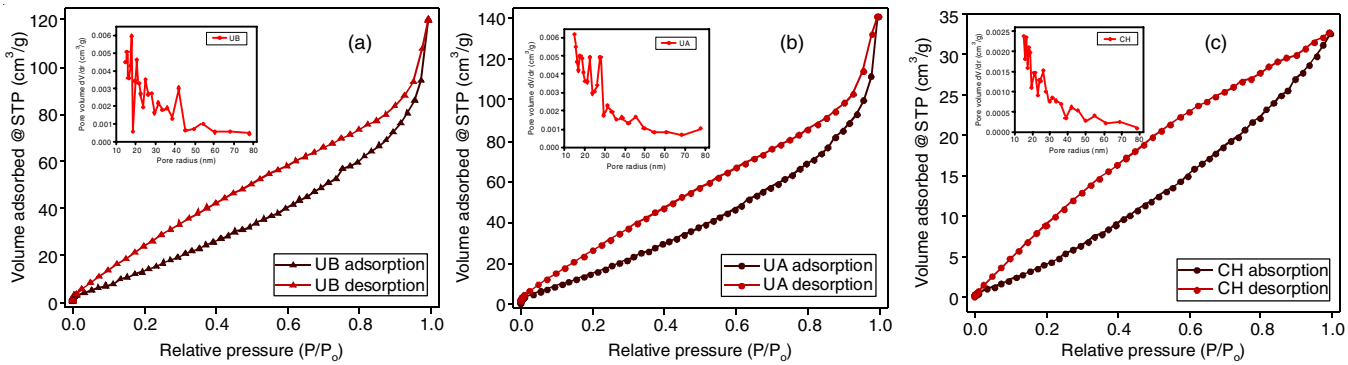

Fig. 7. The hysteresis loop isotherm and BJH pore size and pore volume of the samples; (a) UB adsorption and desorption, (b) UA adsorption and desorption, (c) CH adsorption and desorption

and UA shows type IV isotherm with H3 hysteresis loop except CH, whereas CH shows type III isotherm with H3 hysteresis loop [48,49]. The calculated average BET surface area and BJH average pore size are given in Table-5. The specific surface area of UB is reduced than UA and it indicates the addition of surfactant has increased the specific surface area but the specific surface area of CH is reduced than both samples. The addition of hexamine hydrolyses the reaction and enhances the condensation and agglomeration processes, which in turn forms bigger particles and results in the lower surface area. The calcination process also helps in hydrolysis process as hexamine hydrolyze above 70º [16]. Both the addition of hexamine and calcination process has together resulted in lower surface area.

FTIR studies: The FTIR spectra of the prepared samples portray the mixing-induced interaction between surfactant and photocatalyst. The UB and CH samples were considered for the FTIR analysis based on the sample for comparison and the sample which showed better degradation, respectively. The shoulder peaks at 535 and 480 cm^{-1}, strong peak at 732 and 698 cm^{-1} and medium intense peaks at 1520 and 1526 cm^{-1} for UB and CH respectively and the low intensity peaks for UB is at 1688, 2350 and 2922 cm^{-1} and for CH is at 1727 and 2925 cm^{-1}. The shoulder peaks at 535 cm^{-1} for UB and at 480 cm^{-1} for CH corresponds to the Bi-O stretching [24,50]. The strong intense peak for UB at 732 cm^{-1} ascribed to stretching mode of VO_4 [51] and the medium peak for UB at 1520 cm^{-1} and for CH at 1526 cm^{-1} represents O-H bending mode of the absorbed water molecules [52]. The high intense peak for CH at 698 cm^{-1} attributed to the aromatic C-H bending mode (Fig. 8). The peak at 698 cm^{-1} reveals the presence of hexamine in CH

TABLE-5
CALCULATED SPECIFIC SURFACE AREA, PORE SIZE AND PORE VOLUME OF THE SYNTHESIZED PHOTOCATALYSTS

Sample	Specific surface area (BET analysis)	BJH analysis		
		Specific surface area (m^2/g)	Pore size (nm)	Pore volume (cm^3/g)
Untreated $BiVO_4$ (UB)	81.67	77.78	1.78	0.187
Untreated PVA (UA)	88.08	92.64	1.49	0.222
Calcinated hexamine (CH)	34.46	31.62	1.49	0.054

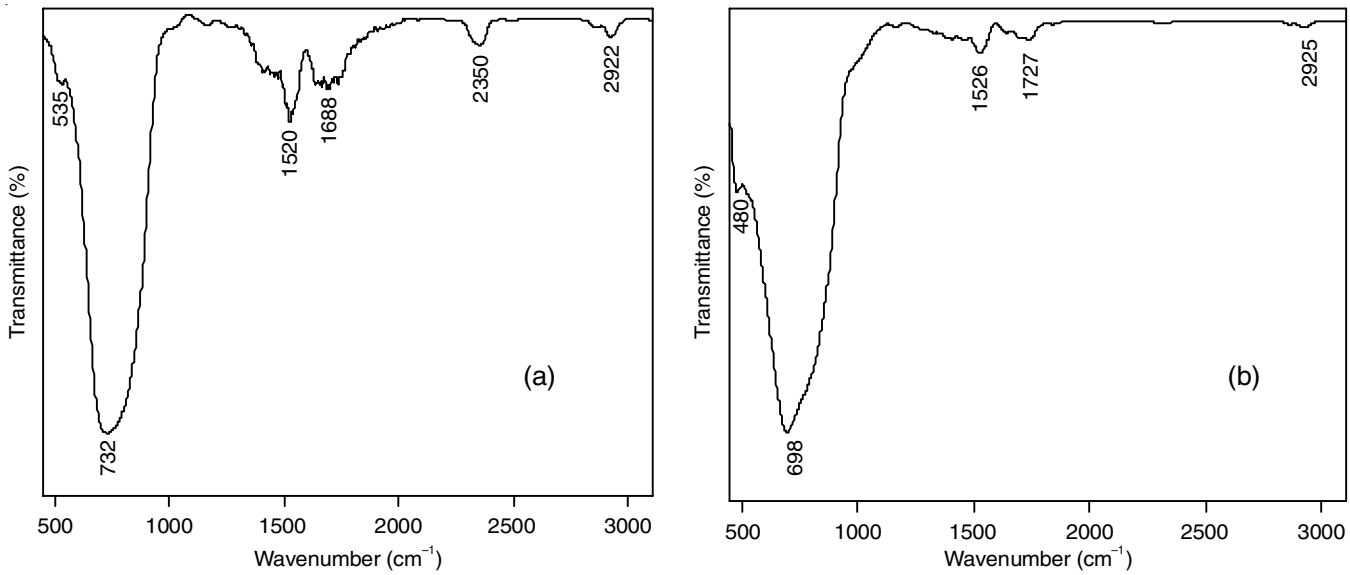

Fig. 8. FTIR spectra of the (a) untreated $BiVO_4$ and (b) calcinated hexamine samples

sample, as hexamine contains long chains of methyl groups [53,54]. The shift in the peaks confirms the presence of $BiVO_4$ and hexamine in the prepared CH sample.

Conclusion

The visible region active semiconductor photocatalyst is synthesized through low temperature solvothermal method. Surface of the prepared samples modified. The CH showed higher photocatalytic efficiency and has lower band gap energy value and lower photoluminescence emission spectra intensity among all the prepared samples. In turn, it indicates that the recombination rate of photoinduced charge carriers plays a vital role in enhancing the degradation efficiency. The CH sample has methylene blue degradation efficiency of 74% in 180 min. The UA sample has the higher surface area but it didn't help in enhancing degradation efficiency. The hexamine present in CH has induced a higher degradation rate after calcination process but other surfactants did not improve the photoactivity after exposing to the high temperature. Thus, the role of hexamine in enhancing the photocatalytic efficiency of $BiVO_4$ is confirmed.

ACKNOWLEDGEMENTS

The authors acknowledge the financial support from DST-SERB through the project EMR/2017/004096.

CONFLICT OF INTEREST

The authors declare that there is no conflict of interests regarding the publication of this article.

REFERENCES

1. Y. Luo, G. Tan, G. Dong, L. Zhang, J. Huang, W. Yang, C. Zhao and H. Ren, *Appl. Surf. Sci.*, **324**, 505 (2015); https://doi.org/10.1016/j.apsusc.2014.10.168
2. Z. Zhao, H. Dai, J. Deng, Y. Liu and C.T. Au, *Solid State Sci.*, **18**, 98 (2013); https://doi.org/10.1016/j.solidstatesciences.2013.01.009
3. Y. Meng, Y. Shen, L. Hou, G. Zuo, X. Wei, X. Wang and F. Li, *J. Alloys Compd.*, **655**, 1 (2016); https://doi.org/10.1016/j.jallcom.2015.09.168
4. X. Gao, Z. Wang, F. Fu and W. Li, *Mater. Sci. Semicond. Process.*, **35**, 197 (2015); https://doi.org/10.1016/j.mssp.2015.03.012
5. Y. Geng, P. Zhang, N. Li and Z. Sun, *J. Alloys Compd.*, **651**, 744 (2015); https://doi.org/10.1016/j.jallcom.2015.08.123
6. W. Liu, L. Cao, G. Su, H. Liu, X. Wang and L. Zhang, *Ultrason. Sonochem.*, **17**, 669 (2010); https://doi.org/10.1016/j.ultsonch.2009.12.012
7. S.M. Thalluri, S. Hernández, S. Bensaid, G. Saracco and N. Russo, *Appl. Catal. B*, **180**, 630 (2016); https://doi.org/10.1016/j.apcatb.2015.07.029
8. X. Meng, L. Zhang, H. Dai, Z. Zhao, R. Zhang and Y. Liu, *Mater. Chem. Phys.*, **125**, 59 (2011); https://doi.org/10.1016/j.matchemphys.2010.08.071
9. Y. Wang, G. Tan, H. Ren, A. Xia, B. Li, D. Zhang, M. Wang and L. Lv, *Mater. Lett.*, **229**, 308 (2018); https://doi.org/10.1016/j.matlet.2018.07.052
10. G. Zhao, W. Liu, J. Li, Q. Lv, W. Li and L. Liang, *Appl. Surf. Sci.*, **390**, 531 (2016); https://doi.org/10.1016/j.apsusc.2016.08.126
11. M. Yang, Q. Yang, J. Zhong, J. Li, S. Huang and X. Li, *Mater. Lett.*, **201**, 35 (2017); https://doi.org/10.1016/j.matlet.2017.04.125
12. H. Fan, D. Wang, L. Wang, H. Li, P. Wang, T. Jiang and T. Xie, *Appl. Surf. Sci.*, **257**, 7758 (2011); https://doi.org/10.1016/j.apsusc.2011.04.025
13. Z. Wu, Y. Xue, X. He, Y. Li, X. Yang, Z. Wu and G. Cravotto, *J. Hazard. Mater.*, **387**, 122019 (2020); https://doi.org/10.1016/j.jhazmat.2020.122019
14. A. Sharma, N. Liu, Q. Ma, H. Zheng, N. Kawazoe, G. Chen and Y. Yang, *Chem. Eng. J.*, **385**, 123765 (2020); https://doi.org/10.1016/j.cej.2019.123765
15. D. Jesuvathy Sornalatha and P. Murugakoothan, *Mater. Lett.*, **124**, 219 (2014); https://doi.org/10.1016/j.matlet.2014.03.100
16. X. Wang and T.T. Lim, *Appl. Catal. A Gen.*, **399**, 233 (2011); https://doi.org/10.1016/j.apcata.2011.04.002
17. H. Chang, E.H. Jo, H.D. Jang and T.O. Kim, *Mater. Lett.*, **92**, 202 (2013); https://doi.org/10.1016/j.matlet.2012.11.006
18. S.I. Eda, M. Fujishima and H. Tada, *Appl. Catal. B*, **125**, 288 (2012); https://doi.org/10.1016/j.apcatb.2012.05.038
19. T. Wang, X.Q. Liu, C.C. Ma, M.B. Wei, P.W. Huo and Y.S. Yan, *Sci. China Technol. Sci.*, **64**, 548 (2021); https://doi.org/10.1007/s11431-020-1611-y

20. P. Ju, Y. Wang, Y. Sun and D. Zhang, *J. Colloid Interface Sci.*, **579**, 431 (2020); https://doi.org/10.1016/j.jcis.2020.06.094
21. Y. Lu, Y.S. Luo, D.Z. Kong, D.Y. Zhang, Y.L. Jia and X.W. Zhang, *J. Solid State Chem.*, **186**, 255 (2012); https://doi.org/10.1016/j.jssc.2011.12.003
22. L. Ye, L. Li, L. Guo, J. Fang, H. Zhao and Y. Jiang, *Mater. Lett.*, **211**, 171 (2018); https://doi.org/10.1016/j.matlet.2017.09.109
23. T.D. Nguyen, V.H. Nguyen, S. Nanda, D.V.N. Vo, V.H. Nguyen, T. Van Tran, L.X. Nong, T.T. Nguyen, L.G. Bach, B. Abdullah, S.S. Hong and T. Van Nguyen, *Environ. Chem. Lett.*, **18**, 1779 (2020); https://doi.org/10.1007/s10311-020-01039-0
24. A. Malathi, V. Vasanthakumar, P. Arunachalam, J. Madhavan and M.A. Ghanem, *J. Colloid Interface Sci.*, **506**, 553 (2017); https://doi.org/10.1016/j.jcis.2017.07.079
25. V. Rajalingam, Ph.D. Thesis, Synthesis and Characterizations of $BiVO_4$ Nanostructured Materials: Application to Photocatalysis, The University of Maine, USA (2015).
26. A.J. Josephine, C.R. Dhas, R. Venkatesh, D. Arivukarasan, A.J. Christy, S.E.S. Monica and S. Keerthana, *Mater. Res. Express*, **7**, 15036 (2020); https://doi.org/10.1088/2053-1591/ab653f
27. M.M. Sajid, N. Amin, N.A. Shad, S.B. Khan, Y. Javed and Z. Zhang, *Mater. Sci. Eng. B Solid-State Mater. Adv. Technol.*, **242**, 83 (2019); https://doi.org/10.1016/j.mseb.2019.03.012
28. J. Yang, N. Sun, Z. Zhang, J. Bian, Y. Qu, Z. Li, M. Xie, W. Han and L. Jing, *ACS Appl. Mater. Interfaces*, **12**, 28264 (2020); https://doi.org/10.1021/acsami.0c06892
29. A. Chihi, M.F. Boujmil and B. Bessais, *J. Mater. Sci. Mater. Electron.*, **30**, 3338 (2019); https://doi.org/10.1007/s10854-018-00607-z
30. H. Jiang, H. Dai, X. Meng, L. Zhang, J. Deng, Y. Liu and C.T. Au, *J. Environ. Sci.*, **24**, 449 (2012); https://doi.org/10.1016/S1001-0742(11)60793-6
31. R. Ran, J.G. McEvoy and Z. Zhang, *Int. J. Photoenergy*, **2015**, 612857 (2015); https://doi.org/10.1155/2015/612857
32. Y. Lin, D. Pan and H. Luo, *Mater. Sci. Semicond. Process.*, **121**, 105453 (2021); https://doi.org/10.1016/j.mssp.2020.105453
33. X. Meng, Z. Li and Z. Zhang, *J. Catal.*, **356**, 53 (2017); https://doi.org/10.1016/j.jcat.2017.09.005
34. M.Q. Pham, T.M. Ngo, V.H. Nguyen, L.X. Nong, D.-V.N. Vo, T.V. Tran, T.-D. Nguyen, X.-T. Bui and T.D. Nguyen, *Arab. J. Chem.*, **13**, 8388 (2020); https://doi.org/10.1016/j.arabjc.2020.05.029
35. C. Qin, H. Liao, F. Rao, J. Zhong and J. Li, *Solid State Sci.*, **105**, 106285 (2020); https://doi.org/10.1016/j.solidstatesciences.2020.106285
36. J. Liu, L. Qiu, M.J. Chang, B. Yuan, M. Sun, S.M. Fan, W.N. Cui, Q. Hui, F.R. Ni, M.Y. Li, Y.Q. Li and Z.M. Luo, *Mater. Chem. Phys.*, **247**, 122858 (2020); https://doi.org/10.1016/j.matchemphys.2020.122858
37. B. Li, G. Tan, M. Wang, D. Zhang, M. Dang, L. Lv, H. Ren, A. Xia, Y. Liu and W. Liu, *Appl. Surf. Sci.*, **511**, 145534 (2020); https://doi.org/10.1016/j.apsusc.2020.145534
38. X. Cao, Y. Gu, H. Tian, Y. Fang, D. Johnson, Z. Ren, C. Chen and Y. Huang, *Ceram. Int.*, **46**, 20788 (2020); https://doi.org/10.1016/j.ceramint.2020.05.048
39. J.P. Deebasree, V. Maheskumar and B. Vidhya, *Ultrason. Sonochem.*, **45**, 123 (2018); https://doi.org/10.1016/j.ultsonch.2018.02.002
40. T. Ahmed, H. Zhang, Y.-Y. Gao, H. Xu and Y. Zhang, *Mater. Res. Bull.*, **99**, 298 (2018); https://doi.org/10.1016/j.materresbull.2017.11.029
41. L. Shan, C. Lu, L. Dong and J. Suriyaprakash, *J. Alloys Compd.*, **804**, 385 (2019); https://doi.org/10.1016/j.jallcom.2019.07.051
42. M. Sun, P. Guo, M. Wang and F. Ren, *Optik*, **179**, 672 (2019); https://doi.org/10.1016/j.ijleo.2018.10.211
43. Q.-Y. Tang, X.-L. Luo, S.-Y. Yang and Y.-H. Xu, *Sep. Purif. Technol.*, **248**, 117039 (2020); https://doi.org/10.1016/j.seppur.2020.117039
44. C. Ravidhas, A. Juliat Josephine, P. Sudhagar, A. Devadoss, C. Terashima, K. Nakata, A. Fujishima, A. Moses Ezhil Raj and C. Sanjeeviraja, *Mater. Sci. Semicond. Process.*, **30**, 343 (2015); https://doi.org/10.1016/j.mssp.2014.10.026
45. H.E.A. Mohamed, B.T. Sone, X.G. Fuku, M.S. Dhlamini and M. Maaza, *AIP Conf. Proc.*, **1962**, 040004 (2018); https://doi.org/10.1063/1.5035542
46. Y. Wang, D. Yu, W. Wang, P. Gao, S. Zhong, L. Zhang, Q. Zhao and B. Liu, *Sep. Purif. Technol.*, **239**, 116562 (2020); https://doi.org/10.1016/j.seppur.2020.116562
47. C. Ma, J. Lee, Y. Kim, W. Cheol Seo, H. Jung and W. Yang, *J. Colloid Interface Sci.*, **581**, 514 (2021); https://doi.org/10.1016/j.jcis.2020.07.127
48. N. Tavker, U. Gaur and M. Sharma, *J. Environ. Chem. Eng.*, **8**, 104027 (2020); https://doi.org/10.1016/j.jece.2020.104027
49. N. Liu, D. Ouyang, Y. Cai and Y. Li, *Ceram. Int.*, **46**, 24534 (2020); https://doi.org/10.1016/j.ceramint.2020.06.240
50. C. Liu and Y. Xu, *Adv. Mater. Res.*, **148–149**, 1469 (2011).
51. R.L. Frost, D.A. Henry, M.L. Weier and W. Martens, *J. Raman Spectrosc.*, **37**, 722 (2006); https://doi.org/10.1002/jrs.1499
52. M.F.R. Samsudin, R. Bashiri, N.M. Mohamed, Y.H. Ng and S. Sufian, *Appl. Surf. Sci.*, **504**, 144417 (2020); https://doi.org/10.1016/j.apsusc.2019.144417
53. K. Vijai Anand, R. Mohan, R. Mohan Kumar, M. Karl Chinnu and R. Jayavel, *J. Exp. Nanosci.*, **9**, 261 (2014); https://doi.org/10.1080/17458080.2012.656708
54. Y. Ning, L.A. Fielding, T.S. Andrews, D.J. Growney and S.P. Armes, *Nanoscale*, **7**, 6691 (2015); https://doi.org/10.1039/C5NR00535C